The EMBO Journal Vol.1 No.5 pp.541 – 547, 1982

# Dimeric arrangement and structure of the membrane-bound acetylcholine receptor studied by electron microscopy

**Horst-Peter Zingsheim*, Dorothea-Charlotte Neugebauer[1], Joachim Frank[2], Wolfgang Hänicke, and Francisco José Barrantes**

Max-Planck-Institut für Biophysikalische Chemie, (Karl-Friedrich-Bonhoeffer-Institut), D-3400 Göttingen-Nikolausberg, FRG

*Communicated by K.Weber*
*Received on 29 April 1982*

**The acetylcholine receptor protein (AChR) from the electric organ of *Torpedo marmorata* is studied in its membrane-bound form by electron microscopy and single-particle image averaging. About half the molecule protrudes from the membrane surface by ~5 nm. The low-resolution 3-D structure of this hydrated portion, including its handedness, can be deduced from averaged axial and lateral projections and from freeze-etched membrane surfaces. In native membrane fragments, a dimeric form of the AChR is observed and the relative orientation of the AChR monomers within the dimer is established. The dimers disappear upon disulfide reduction of the membrane preparations, whereas the average axial projections of the AChR monomer remain unaffected. Since the existence of disulfide bonds linking AChR monomers between their respective δ-subunits is well documented, the approximate position of the δ-subunit within the low-resolution structure of the AChR molecule can be deduced from the structure of the dimers.**

*Key words:* cholinergic receptor/post-synaptic membrane/membrane proteins/*Torpedo marmorata*/image processing

## Introduction

The acetylcholine receptor (AChR) from *Torpedo* electric organ is a membrane protein with an apparent mol. wt. of ~250 000, composed of four types of subunits (α, β, γ, δ; apparent mol. wt. 40 000, 50 000, 60 000, 65 000, respectively; composition 2α, β, γ, δ). The α-subunits carry the binding sites for α-toxins, agonists, nicotinic affinity labels, and inhibitors (for reviews, see Heidmann and Changeux, 1978; Karlin, 1980; Hucho, 1981). Predominantly dimeric forms of AChR have been isolated from unmodified membranes. Dimers arise by disulfide-linkage primarily *via* the respective δ-subunits of the monomers (Chang and Bock, 1977; Hamilton *et al.*, 1977; Sobel *et al.*, 1977; Suarez-Isla and Hucho, 1977). Disulfide reduction converts all oligomeric forms to monomers, a change that is accompanied by cleavage of the δ-δ-bonds, yielding single δ-subunits (Chang and Bock, 1977; Hamilton *et al.*, 1977, 1979; Karlin, 1980).

The functional significance of the dimers remains obscure. No differences in pharmacological properties and ion transport have been detected between monomers and dimers in reconstituted membranes (Anholt *et al.*, 1980; Boheim *et al.*, 1981). Since the AChR arrangement in sub-synaptic membrane regions is remarkably stable (reviews by Barrantes, 1979; Fambrough, 1979), one might conjecture that this is partially mediated by covalent intermolecular linkages. Other factors likely to contribute to this stability include the ν-peptide, a non-receptor peptide of mol. wt. ~43 000 (Rousselet *et al.*, 1979; Barrantes *et al.*, 1980; Lo *et al.*, 1980).

Here we report structural data on the arrangement of AChR in the membrane. The study is based on electron microscopy and single-particle image averaging (Frank *et al.*, 1978; Zingsheim *et al.*, 1980a, 1980b). Images of individual particles are aligned by correlation techniques (Frank, 1980) to maximize the overlap of reproducible, structure-related features. Aligned images are averaged to enhance these features and to suppress random variations. This method reveals the existence of membrane-bound dimers, the orientation of the AChR monomer within the dimer, and the approximate location of the δ-subunit in the AChR monomer.

## Results

### *Identification of AChR dimers in the intact membrane*

Single-particle image averaging was applied to electron micrographs of negatively-stained AChR-rich membrane vesicles (see Materials and methods). The neighbourhoods of individual AChR molecules were initially screened off with circular masks of ~6 nm diameter in order to prevent them from affecting the rotation and translation search on which particle alignment is based. However, these regions were aligned and included in the final averages.

Although the AChR particles in unmodified membranes appear randomly packed to the eye (Figure 1a), image averaging reveals that nearest-neighbour particles are associated pair-wise. This is evident in Figure 1b which represents contours of equal optical density within an averaged field of 25.6 x 25.6 nm. In this image, fine detail was suppressed by low-pass filtering to a resolution of 6.4 nm, while the salient features, i.e., the gross distribution of stain-excluding mass, have been retained. Adjacent to the central density minimum (indicating stain exclusion) there is a second minimum generated by the superposition of neighbouring AChR particles. These particles, which originally fell outside the circular masks, are located at defined positions relative to the central ones. Both minima are of similar size and contrast. Their separation is ~9 nm, corresponding to the nearest-neighbour distance between AChR molecules in native membranes (Barrantes *et al.*, 1980). Upon disulfide reduction of the membranes (using 10 mM dithiothreitol (DTT), see Materials and methods) the second minimum disappears (Figure 1e).

Density contour maps of averaged fields measuring 12.8 x 12.8 nm are shown in Figure 1c,f. These correspond to the central portions of the 25.6 x 25.6 nm fields (Figure 1b,e), but have been low-pass filtered to a resolution of 1.8 nm. They represent axial views of the AChR structure projected along a direction perpendicular to the membrane plane. Their characteristic shape, resembling a horseshoe, remains essentially unaffected by disulfide reduction.

The choice of the indicated resolutions for low-pass filtering was largely governed by an angular uncertainty of about ±15° in the rotational alignment step. As a consequence of this error, the superimposed features are progressively blurred

[1]Present address: Zoologisches Institut der Universität Münster, Hüfferstr. 1, D-4400 Münster, FRG.
[2]Division of Laboratories and Research, New York State Department of Health, Albany, NY 12201, USA.
*To whom reprint requests should be sent.

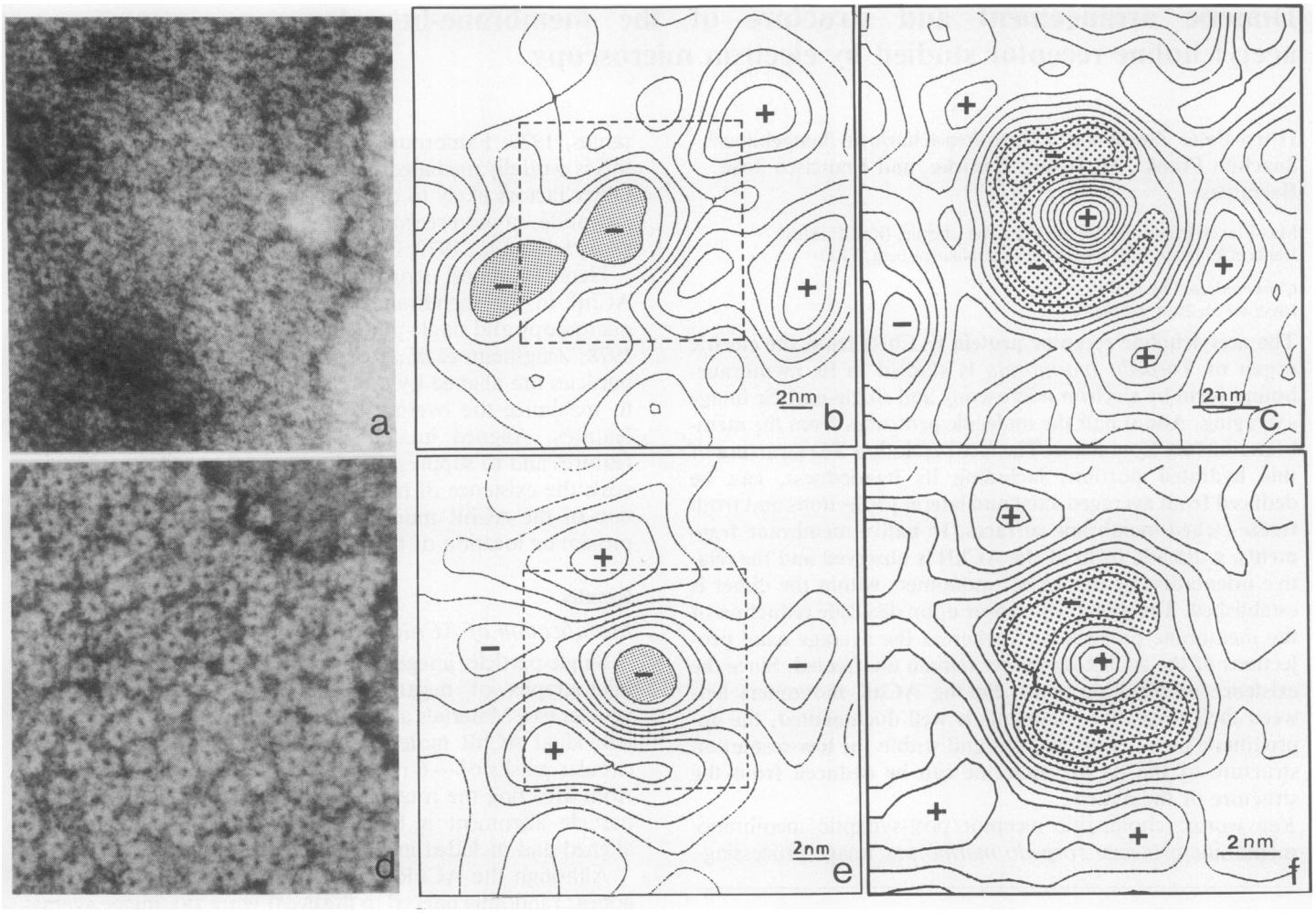


**Fig. 1.** Electron microscopy and image averaging show the dimer arrangement and structure of the membrane-bound AChR. The top row **(a,b,c)** relates to non-reduced (native) membranes. **(a)** is a micrograph of a negatively-stained membrane sheet at a magnification of 500 000 x. Dark regions are due to stain; stain-excluding regions are bright. AChR particles are visualized as 'rosettes' of ~7 nm diameter with a densely stained central pit. Image averaging was applied to small fields centered around individual particles. Only these central particles, with their surroundings screened off by a circular mask of 6 nm diameter were used to find the relative orientations between the particles. Each individual image is represented by optical densities $d_{ik}$ on a square grid of $m^2$ image elements ($i,k = 1,...,m$). In the average image the optical density $\bar{d}_{ik}$ in any image element is the mean of $N$ realizations $d_{ik}^{(n)}$ ($n = 1,...,N$)

$$\bar{d}_{ik} = (1/N)\sum_{n=1}^{N} d_{ik}^{(n)}$$

In **(b)** an average over $N = 20$ individual images is plotted as a contour map of equal values of $\bar{d}_{ik}$, but after low-pass filtering to a resolution of 6.4 nm, thus suppressing all fine detail. The width of the field is 25.6 x 25.6 nm. Relative density minima (stain-exclusion) are marked by $-$; density maxima (stain) are marked by $+$. Shaded areas indicate the most significant density increments in the stain-excluding regions. The presence of the second density minimum adjacent to the central one indicates the association of the AChR particles into dimers. The dashed square (12.8 x 12.8 nm) in the center is presented as a density contour plot in **(c)**, but at a resolution of 1.8 nm. This reveals the typical horseshoe-shaped structure of membrane-bound AChR in axial projection. The bottom row **(d,e,f)** relates to membranes subjected to disulfide reduction using 10 mM DTT. **(d)** is a micrograph (magnification 500 000 x). **(e)** represents a 25.6 x 25.6 nm average over 20 individual images at 6.4 nm resolution. It shows that the dimer arrangement disappears upon disulfide reduction. The 12.8 x 12.8 nm field at 1.8 nm resolution **(f)** shows that disulfide reduction does not significantly affect the typical horseshoe shape.

as their distance from the center increases. The density minima in the stain-excluding region of the central particle are located at a radius of 2.2 nm (see also Figure 1c,f). Here, the azimuthal superposition error is ±0.6 nm, compatible with 1.8 nm resolution (Figure 1c,f). However, at a radius of 9 nm the error is ±2.2 nm, precluding the identification of the stain-filled central pit in the second particle. Therefore the 25.6 x 25.6 nm fields (Figure 1b,e) are presented at a resolution of 6.4 nm.

The averaged neighbourhood features in non-reduced membranes vary somewhat between preparations, but the second density minimum is consistently observed in the same position. Analysis of non-reduced membrane samples after removal of the $\nu$-peptide by alkaline washing (Neubig *et al.*, 1979; Barrantes *et al.*, 1980) also reveals a nearest-neighbour peak in the same position (data not shown).

*Surface relief of the membrane-bound AChR particle*

The surface ['ES' surfaces, Branton *et al.* (1975)] of AChR-rich membranes can be visualized after freeze-etching (Cartaud *et al.*, 1978, 1981; Heuser and Salpeter, 1979). However, the anisotropy of unidirectional shadowing, the random azimuthal orientation of the AChR particles in the membrane, and the variation of the local shadowing angle on the curved membrane faces preclude single-particle averag-

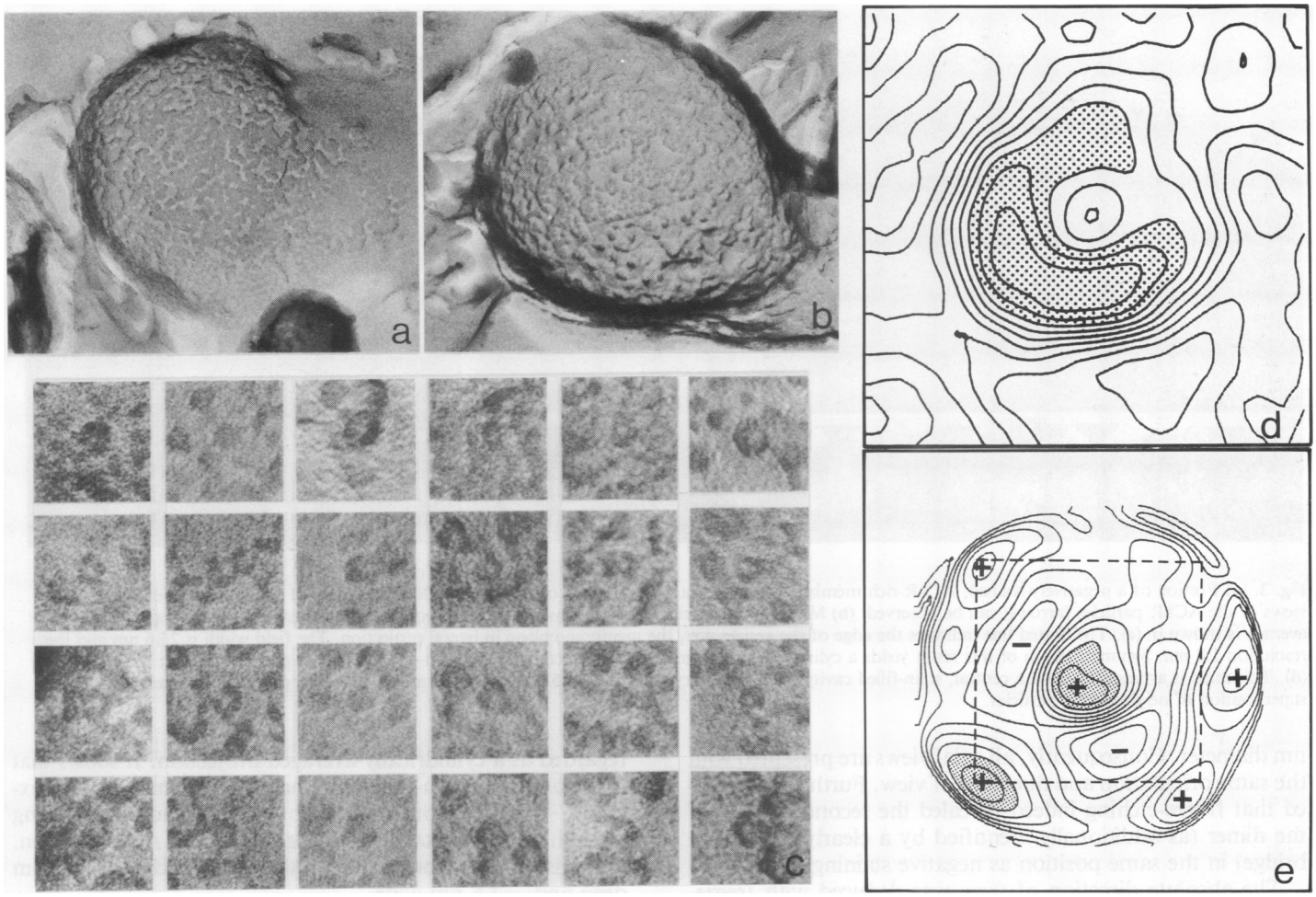


**Fig. 2.** Results of quick-freezing, freeze-etching, and rotary shadowing applied to AChR-rich membrane vesicles. All views projected from the interiors of the vesicles towards their outsides with the metal deposits appearing dark in the micrographs. The vesicles in (**a**) and (**b**) are magnified 100 000 x. The shadowing angle in (**a**) was 45°. The characteristic surface roughness is due to AChR particles exposed by deep-etching. Individual particles can be better discerned using an angle of 17° (**b**). (**c**) presents micrographs of selected particles (shadowing angle 17°, magnification 500 000 x). The particles in the centers of the field were used for alignment and averaging. (**d**) is a contour map of the optical density obtained by averaging 25 particles (resolution of 2 nm, field width 10 nm). Regions of high density, corresponding to metal, have been shaded. This map shows the average distribution of metal deposited on the surface relief structure of the AChR particles. The contour plot in (**e**) presents a larger field of view (25.6 x 25.6 nm) at a resolution of 6.4 nm but with the same orientation as the previous 10 x 10 nm field (dashed square). Density maxima: +; minima: −. It reveals the association of AChR particles into dimers (shaded). The two nearest-neighbour particles appear connected by a 'bridge'. The circular limitation of the field of view is due to the image rotations during alignment and the fact that the original micrographs were cropped.

ing. Isotropy can be obtained with rotary shadowing (Margaritis *et al.*, 1977). Tantalum/tungsten (Ta/W) deposited under an angle of 45° reveals the surface roughness of the deep-etched membranes quite well (Figure 3a), but it remains difficult to discern individual particles. Lowering the shadowing angle to 17° greatly improves the distinction of the particles. However, only small apical regions (e.g., the central areas in Figure 2a,b) of the membrane vesicles are oriented perpendicular to the axis of rotation and can be used to select particles suitable for image averaging (Figure 2c).

The result of image averaging in the form of an optical density contour plot is shown in Figure 2d. At a resolution of 2 nm this represents an average topographic map of the metal piled up on the underlying surface relief structure of the exposed AChR particles. It resembles the horseshoe shape revealed by negative staining (Figure 1c,f). A larger averaged field (25.6 x 25.6 nm) at 6.4 nm resolution (Figure 2e) again reveals the pair-wise association of AChR particles.

In these experiments decoration effects have been minimized by shadowing with Ta/W (Abermann *et al.*, 1972; Zingsheim and Plattner, 1976). This is also evident from the appearance of the high resolution average (Figure 2d). In the presence of decoration effects each of the exposed AChR particles would carry, on average, at least one distinct metal grain on a site of preferential crystallization (but unrelated to the surface profile). Image averaging would serve to enhance these grains. Such a 'high spot' is missing in Figure 2d. This assessment is corroborated by recent results on decoration, shadowing, and image processing of a regular cell wall layer (Baumeister *et al.*, 1981).

*Sidedness and direction of view*

The relative orientations of all averages (freeze-etching and negative staining) were determined by aligning them against one another. This had to include a correlation test for mirror inversion, since the replicas do not always settle on the grids in the same orientation. In order to ensure that only structural information from the central particles contributed, the surrounding regions had been removed by circular masks of 6

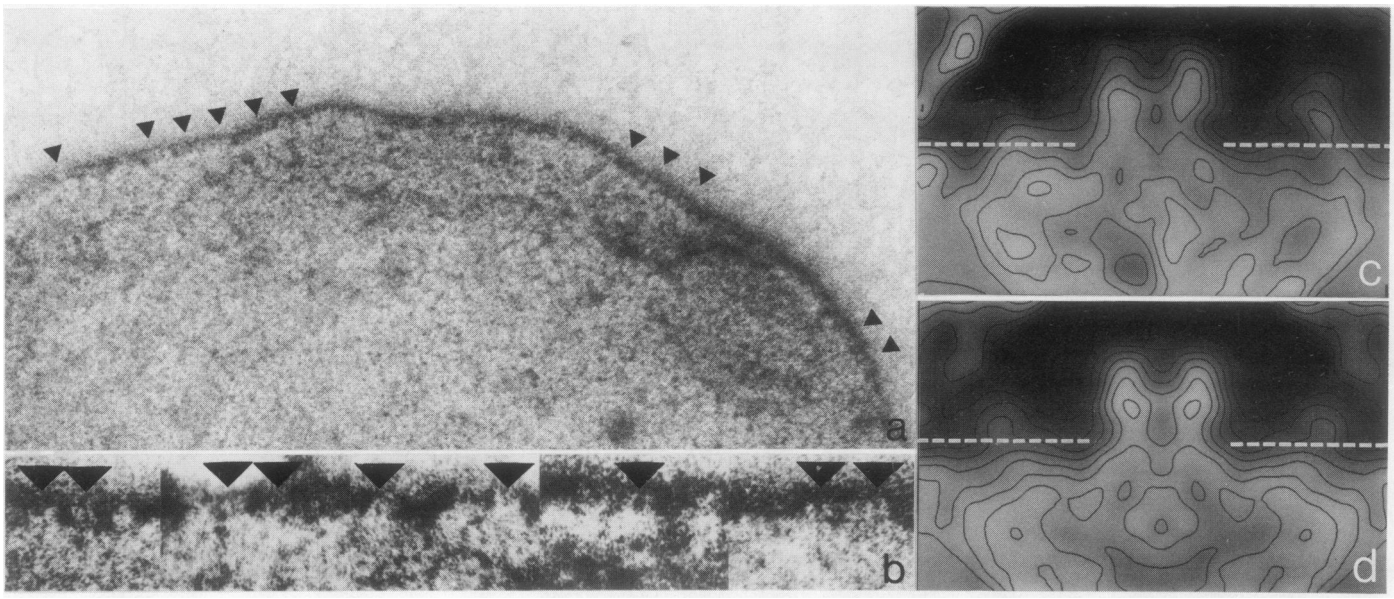


**Fig. 3.** (**a**) Portion of a negatively-stained, AChR-rich membrane vesicle at a magnification of 200 000 x. Along the edges of the flattened vesicles, lateral views of the AChR particles (arrows) can be observed. (**b**) Montage of several such views, as used for subsequent image alignment and averaging. This average is shown in (**c**). The dotted line indicates the edge of the vesicle, i.e., the membrane plane in lateral projection. The field width is 25.6 nm and the resolution 1.8 nm. Symmetrization of this result yields a cylindrically averaged lateral projection of the stain-excluding mass protruding from the membrane (**d**). This mass is arranged around a central, stain-filled cavity. The subsidiary features at 8.5 nm to the left and right of the particle profile arise from the superposition of neighbouring particles.

nm diameter. Consequently, all axial views are presented with the same orientation and direction of view. Further, it emerged that freeze-etching indeed revealed the second particle of the dimer (as additionally identified by a clearly discernible bridge) in the same position as negative staining had done.

The absolute direction of view was deduced with freeze-etched replicas by tilting them in the electron microscope or, alternatively, by observing the refocussing necessary between the apexes of the (convex) ES-faces and the surrounding ice table. This had to be done with each contiguous replica fragment. It followed that the direction of view in Figures 1 and 2 is from the cytoplasmic side of the vesicles. Knowing also the orientation of the negatively-stained grids in the microscope, it was concluded from the correlation test that the extracellular sides of the membrane sheets consistently faced the carbon support film.

A prerequisite of these assignments was the assessment of the sidedness of the membrane vesicles in suspension. The membranes typically used here showed, on average, >90% of their AChR exposed right-side out (see Materials and methods).

*Average lateral view of the AChR particle*

In order to ascertain that the metal deposited by rotary shadowing is indeed piled up on a surface relief structure, it is possible to draw on independent information on the 3-D structure of the AChR. This is available from lateral views of the AChR protein, observed along the edges of negatively stained AChR-rich membranes (Cartaud *et al.*, 1978; Schiebler and Hucho, 1978; Klymkowsky and Stroud, 1979; Figure 3a,b). Alignment (omitting the '180°-decision', see Materials and methods) and averaging of such views leads to the result shown in Figure 3c. This may be symmetrized with respect to an axis perpendicular to the membrane surface (Figure 3d) because information on the azimuthal orientation of the particles is lacking. The symmetrized result can be regarded as a cylindrically-averaged projection. It shows that the protruding stain-excluding mass is ~7 nm wide and extends ~4.5 nm from the membrane, thus accommodating about half of the total mass of the monomeric AChR protein. It is distributed around a central cavity which is ~4.5 nm deep and ~2.5 nm wide.

## Discussion

The use of membrane specimens provides a frame of reference not found in studies of detergent-solubilized material. Complications due to the action of detergents or due to uncertainties with respect to the direction of view (cf., Cartaud *et al.*, 1981; Wise *et al.*, 1981; Holtzman *et al.*, 1982) are avoided. An aspect of general interest is that a study of intermolecular relationships at moderate resolutions was possible by non-crystallographic image averaging without using any *a priori* structural information on the oligomeric organization of the membrane-bound AChR.

Obviously, the reliability of the image averaging procedure, in particular of the rotational alignment step, is a crucial prerequisite. Three methods were used to ascertain the validity of this procedure as applied to images of membrane-bound AChR: a comparison of averages obtained from independent sets of images; a non-parametric statistical test; and the behaviour of the optical density variance of the averages as a function of the total number of images averaged. For a quantitative comparison of two independently obtained averages, the phase residual of their Fourier transforms (Frank *et al.*, 1981b) was computed after masking off the neighbourhood of the particle. The differential phase residual for spacings above ~1.5 nm remains below 45° if averages over ~20 particles are compared. The non-crystallographic test developed on the basis of non-parametric statistical methods established that significant azimuthal density variations (at the 95% level) within distances <2 nm exist in the stain-excluding regions of averages over fully aligned images.

Averages over images merely aligned to by translation show no significant azimuthal contrast variations (Hänicke, 1981). The optical density variance in the stain-excluding region of the average (as an overall measure of contrast variations) was found to be inversely proportional to the number of images averaged (see also Frank *et al.*, 1981b). This indicated that averaging of 20–25 aligned images is sufficient for reducing the noise component of the variance to about a quarter of that due to the reproducible structure (Hänicke, 1981).

Further, the asymmetry of the axially viewed structure (Zingsheim *et al.*, 1980a, 1980b) has also been demonstrated by others, using single particle averaging (Brisson, 1980; Wade *et al.*, 1980) and crystallographic averaging of regular receptor arrays (Kistler and Stroud, 1981; Kistler *et al.*, 1982). Brisson (1980) and Wade *et al.* (1980) determined the relative orientation of the particles directly from their images, rather than from their autocorrelation functions as done here. The results from both alignment methods are in agreement (cf. Steinkilberg and Schramm, 1980). In the present study, freeze-etching and negative staining confirm the asymmetric horseshoe structure of the membrane-bound AChR in axial views, although, in contrast to our earlier procedures (Zingsheim *et al.*, 1980b), we now included in the averages those particles for which the so called '180°-decision' was inconclusive, thus avoiding a bias towards asymmetry (see Materials and methods).

The gain in 3-D information is modest, and restricted to the portion of the AChR exposed on the extracellular face of the membrane vesicles. The average lateral view (Figure 3c,d) suggests that the central pit consists of a shallow outer depression connected to an elongated cavity underneath, with its center of gravity close to the level of the membrane surface. However, the available structural evidence is inadequate to relate the central stain-filled pit to the acetylcholine-induced ion channel (cf., Klymkowsky and Stroud, 1979; Kistler *et al.*, 1982) or to provide clues on the position of physiologically relevant sites on the AChR molecule. Nevertheless, it appears that the customary way of describing the electrostatic situation near pharmacological binding sites or ion channels by assuming a smeared surface charge density on a planar 'membrane surface' (e.g., van der Kloot and Cohen, 1979) may be inapplicable to AChR in view of the fact that about one half of the molecule protrudes into the external medium.

The direct structural evidence for a pair-wise association of AChR particles (dimers) in non-reduced membranes complements previous biochemical information from studies of detergent-solubilized AChR protein. Disulfide reduction known to abolish the δ-δ-linkage (Chang and Bock, 1977; Suarez-Isla and Hucho, 1977; Hamilton *et al.*, 1977, 1979) eliminates the dimeric arrangement in the membrane without significantly affecting the typical horseshoe structure of the AChR monomer. Since the present results are from intact membranes, they considerably strengthen the evidence that the dominating factor stabilizing the membrane-bound dimers are indeed disulfide bonds. This is at variance with recent suggestions that non-covalent interactions predominate (cf., Rüchel *et al.*, 1981).

Although the high contrast of the second particle indicates that only a minor fraction of the AChR is monomeric, this does not imply that the complementary fraction is all dimeric. Oligomeric forms, higher than the dimers, might be present in the intact electrocytes (Hamilton *et al.*, 1979; Heuser and Salpeter, 1979). Thus, some of the twinned particles could be components of such higher oligomers. This precludes the determination of the proportion of dimers relative to all oligomeric forms solely on the basis of the structural data, since the percentage of dimers would be overestimated. Heterogeneity due to the presence of AChR monomers, dimers, and oligomers is a possible explanation for the scarcity of well-ordered AChR arrays as well as for the notorious difficulties in producing them.

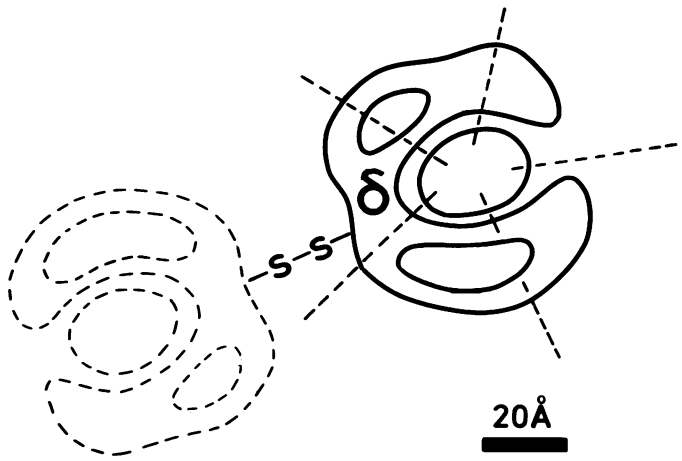


**Fig. 4.** Schematic drawing of the dimeric arrangement of membrane-bound AChR, viewed from the cytoplasmic side of the membrane. The monomers are presented as horseshoe-shaped structures. The segmentation into five sectors is used to indicate in schematic form that each monomer is composed of five subunits. Image processing also revealed that the contact region of the monomers is opposite the 'gap' of the 'horseshoe'. Since the dimers are known to arise from disulfide links between the respective δ-subunits of the monomers, the position of δ within the projection of a monomer can be approximately assigned.

The unambiguous combination of structural and biochemical data at the present level of resolution has been difficult so far because it depends on knowing the position of at least one subunit within the axial projection of the AchR structure. Attempts have been made to compare the ratios of the density peaks with the apparent mol. wts. of the subunits in order to find a reference point (Kistler *et al.*, 1982). However, we believe that, for the δ-subunit, a more direct and convincing assignment is possible. The well documented evidence for disulfide-mediated δ-δ-linkages in AChR dimers isolated from unmodified membranes and the present structural data support the conclusion that the δ-subunits must be located near the region where the monomers join to form dimers. In the average axial projection of the monomer this is the region opposite the 'gap' of the 'horseshoe', as schematically illustrated in Figure 4.

## Materials and methods

*AChR-rich membrane fractions*

The AChR-rich membrane fraction from the electric organ of *T. marmorata* was purified essentially as described (Sobel *et al.*, 1977). Protein content and specific activity were assayed as before (Barrantes, 1980). Specific binding activities ranged from 1.9 to 3.6 nmol α-[$^3$H]bungarotoxin/mg protein. Membrane stock suspensions contained 2–10 mg of protein/ml, 37% (w/w) sucrose, 0.02% $NaN_3$, 1 mM EDTA, 0.1 mM phenylmethane-sulfonylfluoride (PMSF), and 0.1 M Na-phosphate, pH 7.4. Determination of the sidedness of the membrane fragments was performed according to Hartig and Raftery (1979). Aliquots of the stock suspensions were washed once with distilled water by centrifugation in a Beckmann Airfuge (30 s, 20 psi). The pellets were resuspended in distilled water or 0.1 M Na-phosphate, pH 7.4. Typically, volumes of 50–100 μl were used for each experiment. Reduction

with DTT was monitored by gel electrophoresis as described (Hamilton *et al.*, 1979).

*Specimen preparation*

Negatively-stained specimens were prepared as described (Barrantes *et al.*, 1980) on carbon films previously exposed to a 0.1% solution of poly-L-lysine, then washed and dried prior to use. Negative staining was with 1% uranyl formate.

Samples for freeze-etching were made by the copper sandwich method (Gulik-Krzywicki and Costello, 1978) and quick-frozen with a propane jet (Pscheid *et al.*, 1981). For each experiment ~ 50 μl of the stock membrane suspension was diluted into 1.5 ml of a 1.5 mM solution of EDTA pH 7. Samples were washed in this medium four times by low speed centrifugation (Eppendorf centrifuge). The final pellet was resuspended in 100 μl of the same medium. For comparison, a few samples were frozen by the spray-freezing method (Bachmann and Schmitt, 1971). We also compared the two techniques by freezing glycerol/water mixtures and solutions of ferritin in water. The sandwich method worked almost as well as the spray-freezing method (see also Pscheid *et al.*, 1981), but was simpler and required much less membrane material. Freeze etching (2 min at −100°C) was done in a Balzers BAF300 freeze-etch apparatus equipped with a revolving specimen holder. Shadowing with Ta/W (Zingsheim *et al.*, 1970) was done at either 45° or 17°. The metal film thickness was measured with a quartz crystal monitor oriented for normal incidence. The optimal value (contrast *versus* detail) was 0.6−0.7 nm (corrected for the geometry). Standard procedures were used for carbon evaporation, replica separation and cleaning (on 70% $H_2SO_4$), and mounting on copper grids.

*Electron microscopy*

Micrographs of negatively-stained specimens were taken with a high-resolution scanning transmission electron microscope (STEM, Vacuum Generators Ltd., East Grinstead, Sussex, UK) at 60 kV utilizing the elastically scattered electrons (incoherent dark field). We selected sheets of single membranes (ruptured vesicles) in negatively-stained specimens to avoid confusion due to superposition of two membrane layers. The total electron dose on any given specimen area was kept below 1.5 x $10^3$ $e^-$/nm². Micrographs recorded on Ilford FP4 35 mm film (magnification 125 000 x on film) are presented here in reverse contrast (stain dark, stain-excluding regions bright) to facilitate comparison with conventional micrographs of negatively-stained specimens. Micrographs of the freeze-etch replicas were taken at 80 kV with a Philips EM 301 equipped with a goniometer stage.

*Image processing*

Micrographs were digitized with an Optronics rotating drum densitometer at sampling intervals of 50 μm (corresponding to 0.4 nm for negatively-stained specimens and to 0.32 nm for the freeze-etched specimens). For further image processing we used the SPIDER software system (Frank *et al.*, 1981a) implemented on a Digital Equipment PDP 11/60 computer. Half-tone displays and contour plots of computer-stored images were made on a microprocessor-controlled Tektronix storage display (type 611), using a simple dot-matrix method to achieve 8 grey levels. Some half-tone images were also produced on a Perkin Elmer PDS 1010 flatbed densitometer/photowrite unit.

Images were aligned and averaged essentially as described (Zingsheim *et al.*, 1980b). This procedure comprises the following steps: (1) Interactive segmentation of computer-displayed fields (512 x 512 image elements) into small areas of 64 x 64 image elements, each containing several AChR particles, one of them in the center of the field. For each such area, only a central 32 x 32 portion containing a single particle was used for alignment. Within the 32 x 32 area, a circular mask was applied to screen off the surroundings of the central particle, thus preventing random variations of the surroundings from contributing to the alignment. (2) One image is arbitrarily chosen as a reference. (3) All masked images are oriented with respect to the reference image using the autocorrelation function as test function. The orientation search is based on the spacings most consistently represented in the images (2.0 −2.8 nm with staining, Zingsheim *et al.*, 1980b; 2.2−3.5 nm with rotary shadowing). (4) The oriented images are translationally aligned with respect to the reference image. Included in this step is a correlation test ('180°-decision', Zingsheim *et al.*, 1980b) to solve the orientation ambiguity caused by the centro-symmetry of the autocorrelation function. A record is kept of all alignment parameters. (5) All aligned images are averaged by summation. Those with inconclusive '180°-decisions' were not discarded in order to answer criticism of our earlier procedure raised by Brisson (1980), who pointed out that the exclusion of particles with inconclusive 180° tests would bias the result in favour of a non-centrosymmetric appearance. (6) The average thus obtained is used as a reference in further optional (refinement) cycles of alignment, in which steps 3−5 are repeated. (7) The unmasked images (64 x 64 image elements) are aligned (according to the parameters kept on record from steps 3 to 6) and averaged. (8) The averaged images are low-pass filtered to various resolutions and displayed.

## Acknowledgements

We thank Dr. W. Saenger (Max-Planck Institut für Experimentelle Medizin, Göttingen) for the use of his Optronics densitometer. We also thank W. Jahn for the construction of the revolving specimen stage for our freeze-etching apparatus and T. Wronker for his help with the experiments. We thank A. Verschoor for helping with the contouring and filmwriting of the results, and H. Frahm for the photographic work. The support of G. Kessling, J. de Maeyer, and A. di Nicola with many aspects of computer hardware and software is also gratefully acknowledged. Thanks are also due to Drs. D. Henderson, C. Mannella, and A. Verschoor for helpful discussions and advice. This study was supported by a grant from the Deutsche Forschungsgemeinschaft to H.P.Z. (DFG Zi 224/1).

## References

Abermann,R., Salpeter,M.M., and Bachmann, L. (1972) in Hayat,M.A. (ed.), *Principles and Techniques of Electron Microscopy, Biological Applications,* **2**, Van Nostrand Reinhold Company, NY/Cincinnati/Toronto/London/Melbourne, pp. 196-217.

Anholt,R., Lindstrom,J., and Montal, M. (1980) *Eur. J. Biochem.,* **109**, 481-487.

Bachmann,L., and Schmitt,W.W. (1971) *Proc. Natl. Acad. Sci. USA,* **68**, 2149-2152.

Barrantes,F.J. (1979) *Annu. Rev. Biophys. Bioeng.,* **8**, 287-321.

Barrantes,F.J. (1980) *Biochemistry (Wash.),* **19**, 2957-2965.

Barrantes,F.J., Neugebauer,D.-Ch., and Zingsheim,H.P. (1980) *FEBS Lett.,* **112**, 73-78.

Baumeister,W., Kübler,O., and Zingsheim,H.P. (1981) *J. Ultrastruct. Res.,* **75**, 60-71.

Boheim,G., Hanke,W., Barrantes,F.J., Eibl,H.J., Sakmann,B., Fels,G., and Maelicke,A. (1981), *Proc. Natl. Acad. Sci. USA,* **78**, 3586-3590.

Branton,D., Bullivant,S., Gilula,N.B., Karnovsky,M.J., Moor,H., Mühlethaler,K., Northcote,D.H., Packer,L., Satir,B., Satir,P., Speth,V., Staehlin,L.A., Steere,R.L., and Weinstein,R.S. (1975) *Science (Wash.),* **190**, 54-56

Brisson,A. (1980) Thesis, L'Universite Scientifique et Medicale de Grenoble, France.

Cartaud,J., Benedetti,E.L., Sobel,A., and Changeux,J.-P. (1978) *J. Cell Sci.,* **29**, 313-337.

Cartaud,J., Sobel,A., Rousselet,A., Devaux,P.F., and Changeux,J.P. (1981) *J. Cell Biol.,* **90**, 418-426.

Chang,H.W., and Bock,E. (1977) *Biochemistry (Wash.),* **16**, 4513-4520.

Fambrough,D.M. (1979), *Physiol. Rev.,* **59**, 165-227.

Frank,J., Goldfarb,W., Eisenberg,D., and Baker,T.S. (1978) *Ultrasmicroscopy,* **3**, 283-290.

Frank,J. (1980) in Hawkes,P.W. (ed.), *Topics in Physics, vol. 13: Computer Processing of Electron Microscopic Images,* Springer Verlag, Berlin/Heidelberger, pp. 187-222.

Frank,J., Shimkin,B., and Dowse,H. (1981a) *Ultramicroscopy,* **6**, 343-358.

Frank,J., Verschoor,A., and Boublik,M. (1981b) *Science (Wash.),* **214**, 1353-1355.

Gulik-Krzywicki,T., and Costello,M.J. (1978) *J. Microsc.,* **112**, 103-113.

Hamilton,S.L., McLaughlin,M., and Karlin,A. (1977) *Biochem. Biophys. Res. Commun.,* **79**, 692-699.

Hamilton,S.L., McLaughlin,M., and Karlin,A. (1979) *Biochemistry (Wash.),* **18**, 155-163.

Hänicke,W. (1981) Thesis, University of Göttingen, FRG.

Hartig,P.R., and Raftery,M.A. (1979) *Biochemistry (Wash.),* **18**, 1146-1150.

Heidmann,T., and Changeux,J.-P. (1978) *Annu. Rev. Biochem.,* **47**, 317-357.

Heuser,J.E., and Salpeter,S.R. (1979) *J. Cell Biol.,* **82**, 150-173.

Holtzman,E., Wise,D., Wall,J., and Karlin,A. (1982) *Proc. Natl. Acad. Sci. USA,* **79**, 310-314.

Hucho,F. (1981) *Trends Biochem. Sci.,* **6**, 242-245.

Karlin,A. (1980) in Cotman,C.W., Poste,G. and Nicolson,G. (eds.), *The Cell Surface and Neuronal Function,* Elsevier/North Holland Biomedical Press, NY/Amsterdam, pp. 191-260.

Kistler,J., and Stroud,R. (1981) *Proc. Natl. Acad. Sci. USA,* **78**, 3678-3682.

Kistler,J., Stroud,R.M., Klymkowsky,M.W., Lalancette,R.A., and Fairclough,R.H. (1982) *Biophys. J.,* **37**, 371-383.

Klymkowsky,M.W., and Stroud,R.M. (1979) *J. Mol. Biol.,* **128**, 319-334.

Lo,M.M.S., Garland,P.B., Lamprecht,J., and Barnard,E.A. (1980) *FEBS Lett.,* **111**, 407-412.

Margaritis,L., Elgsaeter,D., and Branton,D. (1977) *J. Cell Biol.,* **72**, 47-56.

Neubig,R.R., Krodel,E.K., Boyd,N.D., and Cohen,J.B. (1979) *Proc. Natl. Acad. Sci. USA,* **76**, 690-694.

Pscheid,P., Schudt,C., and Plattner,H. (1981) *J. Microsc.,* **121**, 149-167.

Rousselet,A., Cartaud,J., and Devaux,P. (1979) *C.R. Hebd. Seances Acad. Sci. Paris, Ser. D,* **289**, 461-463.
Rüchel,R., Watters,D., and Maelicke,A. (1981) *Eur. J. Biochem.,* **119**, 215-223.
Schiebler,W., and Hucho,F. (1978) *Eur. J. Biochem.,* **85**, 55-63.
Sobel,A., Weber,M., and Changeux,J.-P. (1977) *Eur. J. Biochem.,* **80**, 215-224.
Steinkilberg,M., and Schramm,H. (1980) *Hoppe-Seyler's Z. Physiol. Chem.,* **361**, 1363-1369.
Suarez-Isla,B.A., and Hucho,F. (1977) *FEBS Lett.,* **75**, 65-69.
Van der Kloot,W.G., and Cohen,I. (1979) *Science (Wash.),* **203**, 1351-1352.
Wade,R.H., Brisson,A., and Tranqui,L. (1980) *J. Microsc. Spectrosc. Electronique,* **5**, 699-715.
Wise,D.S., Wall,J., and Karlin,A. (1981) *J. Biol. Chem.,* **256**, 12624-12627.
Zingsheim,H.P., and Plattner,H. (1976) in Korn,E.D. (ed.), *Methods in Membrane Biology,* **7**, Plenum Publishing Co., NY, pp. 1-146.
Zingsheim,H.P., Abermann,R. and Bachmann,L. (1970) *J. Phys. E: Sci. Instr.,* **3**, 39-42.
Zingsheim,H.P., Barrantes,F.J., Hänicke,W., Neugebauer,D.-Ch., and Frank,J. (1980a) in Brederoo,P., de Priester,W. (eds.), *Electron Microcopy 1980,* **2**, Dutch Society of Electron Microscopy, Leiden, Netherlands, pp. 592-593.
Zingsheim,H.P., Neugebauer,D.-Ch., Barrantes,F.J., and Frank,J. (1980b) *Proc. Natl. Acad. Sci. USA,* **77**, 952-956.